A New Machine Learning-Driven Approach for the Diagnosis of COVID-19: An Ultra Covix Model

Dasari Naga Vinod
Vel Tech Rangarajan Dr Sagunthala R&D Institute of Science and Technology
Adamu Murtala Zungeru
Botswana International University of Science and Technology
S.R.S. Prabaharan (srsprabaharan1611@gmail.com)
SRM Institute of Science and Technology https://orcid.org/0000-0001-8155-0677

Research Article

Keywords: Ultrasound Imaging, COVID-19, Haralick Features, Gradient Mapping, Random Forest, Machine Learning

Posted Date: May 25th, 2022

DOI: https://doi.org/10.21203/rs.3.rs-1642343/v1

Abstract

The rigorous clinical prognosis is ambiguous due to the ongoing global crisis caused by different mutant variations of the prevailing COVID-19 pandemic. Hitherto, various clinical prognosis imaging techniques are suggested to medical practitioners to identify COVID-19 contracted individuals. Herein, we demonstrate an efficient tool aiding ultrasound imaging technique backed by machine learning strategies, which help diagnose COVID-19 infected cases more accurately and efficiently. The latter approach complements CT and chest X-ray imaging methods. Accordingly, our novel method employs gradient mapping and distinct haralick features using the image database (705 Ultrasound Images). We also propose a vivid technique that assists in diagnosing COVID-19 contaminated individuals by examining ultrasound pictures to identify novel coronavirus. The test set of the precision score is analyzed in the light of attainment results viz., accuracy, confusion matrix, and ROC curve by utilizing the GitHub repository, which conforms to their endorsed ultrasound images. Various algorithms are used to examine test sets accompanying 211 clinical image data for classification performance. Interestingly, the article reveals that the multiple classification accuracy of the proposed model has achieved 98.1% accuracy between the COVID-19, normal, and Pneumonia ultrasound image database.

1. Introduction

Until now, SARS-CoV-2 has tainted over 504 million and deceased more than 6.2 million patients globally (https://coronavirus.jhu.edu/map.html (Accessed on 24 April, 2022)). Its long and dispersive hatching time calls for quick, precise, and dependable procedures for early illness analysis to battle the spread [1] effectively. The polymerase chain reaction test (RT-PCR) makes pre-processing time as long as two days [2]. A few articles announced affectability as low as 70% [3], and a meta-investigation assessed the false-negative proportion to be partly 20% throughout the disease [4]. Clinical imaging supplements the analytic cycle that can control further PCR-testing, particularly in emergency circumstances [5]. Computed Tomography (CT) screening is the imaging best quality level for aspiratory infections [6]. It is considered dependable for Coronavirus determination in certain nations, albeit a critical measure of patients illustrates typical CT scans [7]. Notwithstanding, a CT scan is a costly affair and exceptionally illuminating, conveys the considerable danger of cross-contamination to medical practitioners, and requires broad, tedious disinfection [8]. Comparisons of radiography pictures such as Chest X-ray, CT scan, and ultrasound amidst various parameters as shown in Table 1.

Table 1
The analogy of Chest X-ray, CT scan compared with Ultrasound pictures

Chest X-ray	CT Scan	Ultrasound
Chest X-rays are densely utilized for prognosis lung circumstances. They are not well adapted to recognize COVID-19 at initial phases [9].	CT instants a more feasible method for COVID-19 prognosis and has been the most advocated diagnosis method so far [10, 11].	Ultrasound can evince pleural and interstitial thickening, subpleural consolidation phenomena related to alterations in lung structure when the contamination is in the initial phases [12].
Patchy, unclear bilateral alveolar consolidations amidst a peripheral distribution are the significant phenomena to diagnose COVID-19 individuals.	When monitoring COVID-19 patients, Ground glass opacities (GGO) were observed bilateral and consolidated [13].	When monitoring COVID-19 patients, B-lines is a significant phenomenon to diagnose.
Expensive, radiating, and findings were not statistically significant.	It is highly radiating, expensive, and hard to sterilize.	Inexpensive, Portable, easy to sterilize, non-irradiating, safe, and available everywhere.

Recently, ultrasound images, a more generally accessible, cost-effective, protected, and constant imaging procedure, require consideration in the context of intense respiratory problems. Specifically, lung ultrasound (LUS) offers immense benefits in the point-of-care context for the discovery and the executives of patients with intense respiratory problems [14], [15]. In a few cases, it exhibited preferred affectability over chest X-ray in identifying pneumonia [16]. Doctors have lately depicted utilization of LUS imaging in the crisis for determination of Coronavirus afflicted patients [17]. Discoveries propose explicit LUS attributes and imaging biomarkers for Coronavirus patients [18]–[20] might be utilized to both recognize these patients as well as deal with the respiratory adequacy of mechanical ventilation [21]. An extensive scope of appropriateness and generally less cost from ultrasound images is beneficial when patient inflow surpasses the normal medical clinic imaging framework abilities. It is likewise open for low and middle livelihood nations [22]. Nonetheless, portraying ultrasound pictures can be a troublesome errand; furthermore, it leads to errors because of a steep learning curve [23].

The pre-eminent research contributions of this article elucidate as ensuing:

- We have recommended a gradient mapping with haralick image features to recognize the COVID-19, Normal, and Pneumonia individuals using lung Ultrasound pictures.
- We have rigorously examined the ultrasound picture samples aligning to monitor the COVID-19, Normal, and Pneumonia. All the pictures enclose lesions were re-affirmed by qualified radiologists.
- The obtained results are analyzed by utilizing three metrics called accuracy, ROC, and confusion matrix.
- The developed method recommended for the current investigation aids in identifying samples infected with COVID-19 achieved that precision score of 98%.
- The proposed technique achieves 98.1% accuracy for the approximate analysis.

The rest of the article is organized as follows: Segment 2 analyzed the recent lung ultrasound imaging. Section 3 illustrates the image database and pre-processing. In Section 4, we describe the gradient mapping and image segmentation on the image database. Section 5 illustrates the empirical outcomes and discussion with the performance of the method, and lastly, an epilogue is exhibited in Segment 6.

2. Lung Ultrasound Imaging

Lung ultrasound (LUS) is an imaging approach expand by doctors at the point of care to assist in the prognosis and management of acute respiratory defeat. Amidst efficiency coordinating or surpass chest X-rays for most acute respiratory diseases, LUS furthermore absence the radiation and the arduous workflow of CT [24–26]. Additionally, inexpensive battery-regulated approach, LUS can be conveyed extensively in any environment and is admirably adapted for epidemic situations [27]. B lines are the attribute disinfectant characteristics on LUS, initiated by either pulmonary edema or non-cardiac effects of interstitial syndromes. The latter incorporates an extensive list of circumstances that varies from pneumonia, pneumonitis, acute respiratory distress syndrome (ARDS) [28].

For example, clinical imaging can take an essential role in supplementing traditional symptomatic apparatuses from sub-atomic science. Authors in [29] exhibited a few programmed frameworks utilizing machine learning and artificial intelligence procedures, promising exhibitions utilizing CT and X-ray data. In addition, authors in [30] proposed a convolutional neural network, so-called POCOVID-Net, to handle the current computer vision aid. Upon utilizing the convolutional part of VGG-16 and establishing a deep convolutional neural network, it is inferred that it effectively affects different picture types [31]. This mechanism is followed by one hidden layer with 64 neurons by ReLU activation function, dropout of 0.5 [32], and group standardization [33]. The model was assessed in 5-overlay cross approval and stated a grouping exactness of 89% and an affectability to recognize Coronavirus of 96%. The technique exhibits the analytic worth of the gathered information and the pertinence of deep learning for ultrasound pictures.

The dataset described by Born et al. [34] is a freely accessible LUS dataset for Coronavirus that comprises 202 recordings from four classes (Coronavirus, bacterial pneumonia, non-Coronavirus viral pneumonia, and typical images). The authors investigated the worth of machine learning strategies for the differential analysis of lung pathologies on this database. They utilized interpretability strategies for the Spatio-temporal confinement of pneumonic biomarkers to explore the utility of the intended technique considered valuable for human-tuned situations in a blinded report with clinical specialists. Accordingly, they proposed a frame-based approach that accurately recognizes Coronavirus LUS recordings from normal and bacterial pneumonia information deducing the affectability score of 0.90 ± 0.08 and particularity of 0.96 ± 0.04.

Hu, Z. et al. [35] recommended a novel classification network called MCRFNet that uses a multimodal combination, channel, and responsive field regarding arranging lung sonograms. Also, the authors scored the anticipated classes that reflect the level of lung involvement in the patient and assisted specialists

with joining different pointers to survey illness drifts in COVID-19 individuals. The benchmark condition of machine learning models for assessing pixel-level segmentation of Coronavirus imaging biomarkers has been described by Roy et al. [36]. Analyses on the dataset show a satisfactory outcome on all the thought about undertakings, preparing for future exploration on DL for the helped finding of Coronavirus from LUS information.

3. Materials And Methods

3.1 Data Pre-Processing

The dataset utilized in this chore is openly available at GitHub archive [37], which directly resides of around 705 Ultrasound pictures out of these 235 for COVID-19 positive samples, 235 normal individuals, and 235 for Pneumonia individuals. The archive of the image dataset is open for image segmentation techniques, and the entire dataset is confirmed and elucidated, containing the verdict of the Ultrasound images.

Since the images in the dataset are not flexible, Ultrasound pictures enunciate the distinctive range appropriately; we have transformed all the images to a similar range of 224 * 224 pixels. Moreover, the RGB reverting has been imposed, and the consequent input to the suggested method is furnished as 224 * 224 * 3 picture. After that, we applied the gradient mapping and calculated the haralick features for both spatial regions (GLCM, GLDM, and Texture) and frequency region (FFT, DWT) to this model.

3.2 Feature Eradication

We have utilized Texture, Gray-Level Co-Occurrence Matrix (GLCM), Gray Level Distance Method (GLDM), Fast Fourier Transform (FFT), as well as Discrete Wavelet transform (DWT) to measure a combination of 200 features in spatial as well as frequency areas. We estimated the 12 haralick features as in Vinod et al. [41]". The feature extraction method brought over 200 features for each ultrasound image altogether ("12 features arising out of texture and FFT individually, 40 features arising out of GLCM as well as GLDM individually, and 96 features arising out of DWT").

4. Proposed An Ultra Covix Technique

The training system utilizes "an anaconda-Jupyter notebook by tensor flow" mechanism as elucidated by Vinod et al. [41] to train the broad image dataset. Access to the required libraries was done at the starting phase to connect the code from other components. After that, uploading the image dataset to the path, then applying gradient mapping to the images and extracting the features with the help of spatial and frequency regions viz. "GLDM, FFT, DWT, GLCM as well as Texture" for disjuncture. Finally, we have concatenated all 200 haralick lineaments in both the regions and called an Ultra Covix technique to identify the COVID-19 individuals facilitated by the random forest algorithm, as exhibited in Fig. 2. The image pre-processing process as exhibited in algorithm-1 and feature eradication of the pictures are

illustrated in algorithm-2. Finally, categorization and efficiency measures of the system are exhibited in algorithm-3 for an Ultrasound image dataset amid multiple classifications.

Algorithm 1: Lung Ultrasound Image database for Pre-processing
Input : Input Image I(e, f, g) $_{(e, f, g) \quad (1,2,....n)^3, e = f = g}$
Output : Output Image O(e, f, g) $_{(e, f, g) \quad (1,2,....n)^3, e = f = g}$
Begin
For each Input image, I do
For {e, f, g} = 1 to n do
Apply gradient mapping for producing the heat maps using Eq. (5) on the sample images
Convert input image I into gray and resize the image with 224*224
Apply min-max normalization and return the output image(O)
End For
End For
Where e, f, g are the labels in the ultrasound picture, dataset and n are the pictures' sum.

Algorithm 2: Lung Ultrasound Image database for Feature Extraction
Input : Input Image O (e, f, g) $_{(e, f, g)\ \ (1,2,....n)^3}$, e = f = g
Output : Ultra Covix model
Begin
For each Input image O, do
For {e, f, g} = 1 to n do
IF file ← e, Then

Label ← 0
ELIF file ← f,
Label ← 1
ELSE
Label ← 2
ENDIF

End For
End For
F ← {Calculating features on input image O (12 Haralick features)}
Textual, T ← Compute F on the input image, O FFT, F ← Compute F on the input picture, O DWT, d1 ← Compute F on the input image, O DWT, d2 ← Compute F on Approximation of d1 image D ← d1 + d2 GLDM, G ← Compute F on input image O in four directions using Eq. (6) GLCM, g ← Compute F on input image O in four directions Ultra Covix model $\leftarrow \sum_{i=1}^{n}\{\mathbf{T}, \mathbf{F}, \mathbf{D}, \mathbf{G}, \mathbf{g})\}$ ε O (Total F=200) Save the model

Algorithm 3: Train the Lung Ultrasound Image dataset felicitated by Ultra Covix model
Input : Ultra Covix model, number of instances = 100, Testing ratio = 30%, Training ratio = 70%, number of trees = 100, Classifier = Random Forest.
Output: Confusion Matrix, Visualization, Performance metrics, Training and accuracy loss.
Begin
For Input Ultra Covix model, do
x = concatenate {(e(F), f(F), g(F))} ε $(1,2,\ldots n)^3$ (inputs) y = concatenate {(e(F), f(F), g(F))} ε $(1,2,\ldots n)^3$ (target labels)
End For

4.1 Gradient Visualization

Gradient mapping is a prominent mechanism for the model. It elucidates that it employs comprehensive average pooling and admits to estimating class-specific heat maps that reveal the discriminative areas of the image that provokes appropriate class activity of interest [38]. Gradient mechanism on a basic inference that the eventual count X^d for a specific category d can be exhibited as a linear combination of its comprehensive average pooled last convolutional layer feature maps B^i.

$X^d = \sum_i g_i^d . \sum_m \sum_n B_{mn}^i$ (1)

Respective spatial location (m, n) in the category-specific saliency map S^d is then estimated as:

$$S_{mn}^d = \sum_i g_i^d . B_{mn}^i \text{(2)}$$

S_{mn}^d, precisely associates with the relevance of a specific spatial location (m, n) for a particular category d and thus objectives as perceptible information of the category predicted by the network. Class activation map evaluates these weights g_i^d by training a linear classifier for each category d utilizing the activation maps of the last convolutional layer accomplished for a given picture, the weights g_i^d for an appropriate feature map B^i and the category d is equivalent to:

g_i^d = Y. $\frac{\partial X^d}{\partial B_{mn}^i} \forall \{m, n | m, n \in B^i\}$ (3)

Where Y is a fixed, utilizing gradients flowing from output category into activation maps of last convolutional layer as neuron importance weightsg_i^d.

$$g_i^d = \frac{1}{Y} \sum_m \sum_n \frac{\partial X^d}{\partial B_{mn}^i} \text{(4)}$$

The class selective saliency maps for a given image, S^d are then estimated as a linear combination of the forward activation maps, ensued by a ReLU activation function. Each spatial aspect in the saliency map S^d is then calculated as:

$$S_{mn}^{d} = ReLu\left(\sum_i g_i^d . B_{mn}^i\right) \text{ (5)}$$

For medical applications, gradient mapping or their conjecture Grad-CAMs [39] can afford relevant decision support by deciphering either a mechanism that detects its positioning on precise pathological arrangements. Furthermore, gradient mapping can guide medical practitioners and point to descriptive arrangements, notably compatible in time-sensitive or insight-sensitive positions. The gradient visualization provides various segmentation approaches like FFT, Wavelet, GLCM, GLDM, and Texture to diagnose COVID-19 individuals that distinguish to various diagnosis methods and conclusions were initiate better performance by observation.

Figure 3. exhibits the gradient mapping technique on the lung ultrasound images with and without COVID-19. For a more visual evaluation, we estimated the point's maximal activation of the gradient mapping of each class (COVID-19, Normal, and Pneumonia) and all the database pictures. While the heat maps are adequately scattered across the probe, pneumonia-associated features localized at the center and bottom, notably related to COVID-19 and Normal patterns.

4.2 FFT Based Segmentation

Fast Fourier Transform (FFT) gauges the discrete Fourier transform (DFT) just as its reverse. The FFT advancement is used to novitiate a digital signal (d) between range (r) from the time locale into a recurrence district (R), contemplating the amplitude of vibration dependent on its encouraging among the recurrence as the sign arises.

The recurrence range vector is parted into different frequencies to robotize the selection technique for the sensitive frequencies to the deficiency under investigation. The normal of every degree is then taken as a tangible viewpoint for the substance. In FFT, we have determined the 12 measurable elements in all pictures.

4.3 GLCM Based Disjuncture

Gray Level Co-occurrence framework (GLCM) is a scientific cycle comprehensively used to portray pictures and essentially for Second Harmonic Generation (SHG) collagen image grouping. This framework contemplates the spatial association among the image pixels at a specific point. Ordinarily, it is estimated for four directions at a specific range. Over this lattice, a textural feature is persistent. Routinely, different directions are differentiated or found in the center value to get an original estimation limit.

The co-occurrence lattice is officially characterized as the likelihood of grey level p happening in the neighborhood of another grey level q at a distance f in course C, S (p, q | f, C), where f is a removal vector,

f = (Δc, Δi). The direction C is one of the eight directions. It usually is disregarded the distinction between reverse directions, and afterward, symmetric likelihood lattices can be utilized uniquely for four directions 0 , 45 , 90 , and 135 . Accurate estimates extricate picture highlights from this lattice. In GLCM, we have determined the initial ten measurable provisions in four spatial areas for entire pictures.

4.4 GLDM and Texture Based Segmentation

Texture as a picture feature is incredibly significant in many picture handlings, just as computer vision applications. An exhaustive study on surface assessment in the image refining study uncovered the fundamental focus on hand, division, and association. The surface features have been used in different applications, for example, satellite and aeronautical picture assessment, clinical picture examination for recognizing varieties from the anomalies, recently in picture recuperation using the surface as a descriptor. This part gives an approach to depicting the surface using a multi-band deterioration of the picture with application to portrayal, segmentation, object acknowledgment, and image recovery. In the surface examination, we have determined the twelve factual provisions from every one of the pictures.

Grey level difference method thickness capacities with regards to the pre-handled grey picture. This procedure is used for eliminating the whole surface features of a high-level picture. Contrast is portrayed as the change in thickness among the most essential and least thickness stages in a picture. In this way, the local assortments are on the grey level. We have determined the initial ten measurable components in four spatial areas amid range, t = 8 from reference and neighbor pixels (a, b) in overall pictures in the data set.

$$u(a, b) = |v(a, b) - v(a, b + t)| \quad (6)$$

Where v is the input picture, u is the output of picture v, t is the distance for GLDM estimation.

4.5 Wavelet-Based Segmentation

A discrete wavelet transform is consistently portrayed as a non-excess tried CWT. The wavelet change intends to abode a discrete-time plan, x(s), as many (wavelet) coefficients. These coefficients are examined from a CWT, commonly to produce a balanced set of reasonable limits. Wavelet arrangements are plentiful, with fluctuating characteristics. This part, though, is restricted to the circumstance of even wavelets with little assistance.

There are a couple of similar viewpoints from which the wavelet can be regarded. Here we choose to examine the wavelet through the possibility of a channel bank. A few finite impulse response (FIR) channels with N coefficients are portrayed. One of these channels is high-pass, while the second is low-pass; the two channels cut on/off at an enormous part of the examining repeat. Wavelet transform can be described by using these channels as well as employing them recursively. The channels are first employed to the input time course of action to produce low-pass and high-pass sections, X1(s) and X2(s), independently:

$X_1(s)=\sum_{l=0}^{N-1} e_l y(s-l)$ (7)

$X_2(s)=\sum_{l=0}^{N-1} f_l y(s-l)$ (8)

Wheree_l, and f_l, are the coefficients of the low-pass and high-pass filters individually. It is entirely conventional to assemble the high-pass channel subject to the low-pass channel, which is broadly adapted using the turning flip arrangement, so the two plans of channel coefficients are associated through:

$$f_l = (-1)^l e_{M-l}$$

9

The yield of the two filters is a vast segment of the input progression transmission capacity, such that X1(s) includes the lower recurrence range and X_2(s) the upper band. The yields of every one of the channels are a high ratio of the first data transmission of X(s) to provide these double cross arrangements enclose colossal information.

Here, we have done two-way sequential coefficient operations such as (Coefficient Approximation) CA1, (Coefficient Horizontal) CH1, (Coefficient Vertical) CV1, and (Coefficient Diagonal) CD1 as shown in Fig. 4. Repeatedly CA1 determined more wavelet coefficients; for instance, CA2, CH2, CV2, and CD2 for each successive coefficient, we have determined the twelve factual features.

4.6 Implementing Random Forest Algorithm

Random Forest is a supervised learning technique employing for categorization as well as regression disputes. Nevertheless, it is primarily using for categorization disputes. We envisage that a forest involves trees, and more trees indicate a highly effective forest. Generally, the random forest technique generates decision trees on data samples and finally gets the forest from every one of them eventually chooses the finest explication by choosing. A group mechanism is preferable to an individual decision tree since it curtails the over-fitting by averaging the result. The mechanism of the random forest classifier is exhibited in algorithm-4.

Algorithm 4: Random Forests for Regression or Classification

1. For r = 1 to S:
   i. Construct a bootstrap model K of size L from the training data.
   ii. Develop a random-forest tree F_r to reboot the data by iteratively recurrent the ensuing stages for every terminal node until the tiniest node size l_{min} is attained.
      (a) Choose n variables at random from the q variables.
      (b) Select the finest variable/split-point between the n.
      (c) Divide the node into two daughter nodes.
2. Result of the collection of trees $\{\boldsymbol{F}_r\}_1^S$.

To accomplish a prophecy at a new point y:

Regression: $\boldsymbol{\phi}_{rf}^{S}(\boldsymbol{y}) = \frac{1}{S}\sum_{r=1}^{S}\boldsymbol{F}_r(\boldsymbol{y})$.

Classification: Consider $\beta_r(y)$ to be the class prophecy of the r^{th} random forest tree.
$\boldsymbol{\beta}_{rf}^{S}(\boldsymbol{y})$ = majority vote $\{\boldsymbol{\beta}_r(\boldsymbol{y})\}_1^S$.

End For

Where S is the number of trees, $\boldsymbol{F}_r$ is the r^{th} tree and β_r is the class value for r^{th} tree.

The Random Forest technique, an ensemble machine learning mechanism commonly famous for its better accomplishment over various machine learning classifiers, was adopted for this system. We elicited random forest techniques on subdivisions of COVID-19 samples, characterize them by Normal as well as Pneumonia samples. The number of trees and the selected number of samples are 100 is utilized in the random forest technique to refine if the batch prophecy is being executed.

5. Outcomes And Discussion

Although training the model, the testing samples obtained nearly 1.9% loss score and 98.1% accuracy in lung ultrasound pictures with 100 epochs. The loss rate indicated a strong match among training and testing, affirming that this model is not experiencing overfitting or underfitting in the lung ultrasound image database. Then, we attained a Receiver Operating Characteristics (ROC) curve to estimate the affectability of our model, as exhibited in Fig. 5. (a, b, c). An examination of lung ultrasound pictures of COVID-19 with non-COVID-19 and normal indicated that this system achieves a 97% precision score and 98% recall score when examined on a test set of 211 ultrasound pictures, as exhibited in Table 2. Thus, we have reached the rigorousness of the machine learning classifier, which provides expeditious results amidst both slices of training and testing datasets.

The depiction evaluates utilized for recognizing the COVID-19, Normal, and Pneumonia pictures are ensuing. Where T.P. indicates True Positive, T.N. represents True Negative, F.P. indicates False Positive, and F.N. represents False Negative.

Accuracy = $\frac{T.P.+T.N.}{T.P.+F.P.+F.N.+T.N.}$ (10)

Precision = $\frac{T.P.}{T.P.+F.P.}$ (11)

Recall = $\frac{T.P.}{T.P.+F.N.}$ (12)

Matthews Correlation Coefficient (MCC) = $\frac{(T.P.XT.N.)-(F.P.XF.N.)}{\sqrt{(T.P.+F.P.)(T.P.+F.N.)(F.P.+T.N.)(T.N.+F.N.)}}$ (13)

F-Measure = $\frac{2*Precision*Recall}{Precision+Recall}$ (14)

Table 2
Attainment measures for the recommended mechanism: Ultrasound Images

Label	Precision	Recall	F-Measure	MCC
COVID-19	0.97	0.98	0.98	0.96
Normal	0.98	0.97	0.97	0.96
Pneumonia	0.98	0.98	0.98	0.97

Table 3
Confusion Matrix for foreseeing 211 test samples by COVID-19, Normal and Pneumonia

	COVID-19	Normal	Pneumonia	Image count
COVID-19	73	1	0	74
Normal	1	70	1	72
Pneumonia	1	0	64	65
			Total	211

Table 3. shows the Confusion matrix for the ultrasound picture dataset. The performance comparison in five methods with haralick features is calculated according to accuracy and kappa values, as shown in Table 4. The proposed ultra covix technique has good foresee than various methods associated with COVID-19 as well as normal. It shows the implication of achieving such a recurrence area and concludes that those lineaments are appropriate to recognizing COVID-19 identification in ultrasound pictures. The proposed model improves 19.5%, 10.9%, 4.3%, 10.9%, and 7.6% accuracy, correlated with Texture, FFT, DWT, GLCM, and GLDM feature eradication methods. The proposed method gives a recall of 98%, MCC of 96%, the precision of 97%, and F-Measure of 98% amid COVID-19 is the target class.

Table 4
Comparison of the proposed model with five various categories

Methods	Accuracy (%)	Value of Kappa
Texture (t)	78.6	0.68
FFT (f)	87.2	0.8
DWT (d)	93.8	0.9
GLCM (gc)	87.2	0.8
GLDM (gm)	90.5	0.85
Proposed Ultra Covix technique (t + f + d + gc + gm)	**98.1**	**0.96**

Table 5
Performance metrics of various machine learning classifiers on Ultrasound image database by Train (70%) – Test (30%) split mechanism

Machine Learning Classifiers	Accuracy (%)
SVM	46.9
Naive Bayes	51.1
Decision Tree	86.2
Random Forest	**98.1**
Logistic	93.8

Additionally, we have enforced various machine learning classifiers and deep learning techniques to classify the COVID-19 samples. The Random Forest technique gives high accuracy when correlated to various techniques, as illustrated in Table 5, although the deep learning mechanism gives 84.8% accuracy in the Ultrasound image dataset. We have enforced various training as well as testing splitting methods, as illustrated in Table 6. Furthermore, we have enforced the cross-validation method, as shown in Table 7. Splitting mechanism with training set by 70% and testing set by 30% obtained high accuracy with a large number of pictures in the testing set compared with cross-validation technique and other separation ratios.

Table 6
Analogy of distinct ratios of Train-Test separation on Ultrasound image database

Train – Test separation by Random Forest Algorithm	Sample Ratio (Train – Test)	Accuracy (%)
90% – 10%	635–70	98.5
80% – 20%	564–141	97.1
70% – 30%	**494–211**	**98.1**
60% – 40%	423–282	97.8
50% – 50%	352–352	97.7

Table 7
Comparison of various folds by Cross-Validation mechanism with Random Forest Classifier

Cross-Validation	Accuracy (%)
Fold – 5	97.5
Fold – 10	98.2
Fold – 15	98
Fold – 20	97.8
Fold – 25	98.1
Avg.	**97.9**

Table 8
Distinct deep learning techniques enforced to recognize COVID-19 individuals through Ultrasound pictures.

Reference	Mechanism	Accuracy (%)
Gabriel et al. [30]	POCOVID-19	89
Jannis et al. [34]	VGG	87.8
Roy et al. [36]	U-Net	94
	Deep v3 + with U-net and U-net++	96
Rahimzadeh et al. [32]	NASNET Mobile	62.5
Zhaoyu Hu et al. [35]	MCRFNet	97.7
Proposed Method (Ultra Covix model)	**Gradient mapping + Haralick features**	**98.1**

POCOVID-19 model recommended by Gabriel et al. [30] improves the classification execution by 5-fold cross-validation. The experimental outcomes exhibit that the recommended system has accomplished 89% accuracy and 96% sensitivity. A VGG positioned model endorsed by Jannis et al. [34] has obtained an accuracy of 87.8%. An ensemble Deep v3 + with U-net and U-net + + suggested by Roy et al. [36] enhances the overall performance by separating multiple features utilizing Xception and ResNet50V2 networks. The suggested mechanism obtained reliability of 96%. Rahimzadeh et al. [32] proposed that NASNET mobile has achieved an accuracy of 62.5%. An MCRFNet model proposed by Zhaoyu Hu et al. [35] performed an accuracy of 97.7% with binary classification. Table 8 illustrates various methods enforced in the picture dataset to determine COVID-19 individuals with accomplishment measures likely accuracy (%) for subjective study. We have enforced the ultra covix mechanism in the unchanging image dataset from the GitHub archive, utilized by the various recent investigations. We have entirely utilized the machine learning mechanism as well as obtained high performance with a balanced image database than the various investigations.

6. Conclusion

A fiction lumen segmentation of the COVID-19 prognosis using lung ultrasound images combining gradient mapping and various haralick features has been proposed. Gradient visualization recognizes exceptions and highlights the critical regions of the image to superimpose, which are utilized to hone the segmentation techniques. The mechanism is autonomous of any user characterized boundaries, making it reasonable for distinctively arranged lung ultrasound pictures. Super-pixels are recognized as well as aggregated dependent on the surface and spatial data and are divided. The mechanism concentrates on the overall design of an image and hence gives comprehensive ideal outcomes. The proposed mechanism accomplishes the best-in-class execution at a lot lesser outperforms POCOVID-Net, COVID-Net, and various mechanisms. The technique is mechanized and attempted in a broad arrangement of 705 pictures, and the outcomes are exact. Hence our mechanism can turn into an effective procedure for diagnosing COVID-19 with lung ultrasound picture segmentation. The recommended technique can recognize a COVID-19 positive sample amidst a precision rate of 0.97 as well as a recall score of 0.98. We have had a small database size and achieved an accuracy of ~ 98% for multiclass with an aide of ultrasound pictures. The results achieved are imperative for the timely disclosing to the readers of the benefits of ultrasound images in the context of COVID19, and future examinations will deal with large databases.

Declarations

Conflict of interest None

Ethical Approval and Consent to participate Not Applicable

Consent for publication Not Applicable

Availability of supporting data https://github.com/DASARINAGAVINOD/Covid-19_Ultrasound

Funding None

Competing Interests None

Authors' contributions Dasari Naga Vinod – Formulated, co-designed and performed the simulation work and co-written the manuscript. **Adamu Murtala Zungeru** – Co-designed and co-written the manuscript. **S.R.S. Prabaharan** – Senior author who conceived the idea and co-written the manuscript.

References

1. Li Q, Guan X, Wu P, Wang X, Zhou L, Tong Y, Ren R, Leung KS, Lau EH, Wong JY et al (2020) Early transmission dynamics in Wuhan, China, of novel coronavirus–infected pneumonia. N Engl J Med 382:1199–1207
2. Mei X, Lee HC, Diao Ky, Huang M, Lin B, Liu C, Xie Z, Ma Y, Robson PM, Chung M et al (2020) Artificial intelligence– enabled rapid diagnosis of patients with COVID-19. Nat Med 26:1224–1228
3. Kanne JP, Little BP, Chung JH, Elicker BM, Ketai LH (2020) Essentials for radiologists on COVID-19: An update—Radiology scientific expert panel. Radiology 296:E113–E114
4. Kucirka LM, Lauer SA, Laeyendecker O, Boon D, Lessler J (2020) Variation in False-Negative Rate of Reverse Transcriptase Polymerase Chain Reaction–Based SARS-CoV-2 Tests by Time Since Exposure. Ann Intern Med 173:262–267
5. Dong D, Tang Z, Wang S, Hui H, Gong L, Lu Y, Li H (2020) The role of imaging in the detection and management of COVID-19: a review. IEEE Rev Biomed Eng 14:16–29
6. Bourcier JE, Paquet J, Seinger M, Gallard E, Redonnet JP, Cheddadi F, Garnier D, Bourgeois JM, Geeraerts T (2014) Performance comparison of lung ultrasound and chest x-ray for the diagnosis of pneumonia in the ED. Am J Emerg Med 32:115–118
7. Fang Y, Zhang H, Xie J, Lin M, Ying L, Pang P, Ji W (2020) Sensitivity of chest CT for COVID-19: Comparison to RT-PCR. Radiology 296:E115–E117
8. Yang Y, Huang Y, Gao F, Yuan L, Wang Z (2020) Lung ultrasonography versus chest CT in COVID-19 pneumonia: A two-centered retrospective comparison study from China. Intensive Care Med 46:1761–1763
9. Chen N, Zhou M, Dong X, Qu J, Gong F, Han Y, Qiu Y, Wang J, Liu Y, Wei Y et al (2020) Epidemiological and clinical characteristics of 99 cases of 2019 novel coronavirus pneumonia in wuhan, china: a descriptive study. The Lancet 395(10223):507–513
10. Bao C, Liu X, Zhang H, Li Y, Liu J (2020) COVID-19 computed tomography findings: a systematic review and meta-analysis. J Am Coll Radiol 17(6):701–709

11. Elaine YP, Lee M-Y, Ng, Pek-Lan Khong (2020) COVID-19 pneumonia: what has ct taught us? Lancet Infect Dis 20(4):384–385
12. Buonsenso D, Pata D, Chiaretti A (2020) COVID-19 outbreak: less stethoscope, more ultrasound.The Lancet Respiratory Medicine, 8(5), e27
13. Kanne JP (2020) "Chest CT findings in 2019 novel coronavirus (2019-nCoV) infections from Wuhan, China: key points for the radiologist." :16–17
14. Mojoli F, Bouhemad B, Mongodi S, Lichtenstein D (2019) “Lung ultrasound for critically ill patients,” Amer. J. Respiratory Crit. Care Med., vol. 199, pp. 701–714, Mar.
15. Raheja R, Brahmavar M, Joshi D, Raman D (2019) “Application of lung ultrasound in critical care setting: A review,” Cureus, vol. 11, no. 7, p. e5233, Jul.
16. Amatya Y, Rupp J, Russell FM, Saunders J, Bales B, House DR (Dec. 2018) Diagnostic use of lung ultrasound compared to chest radiograph for suspected pneumonia in a resource-limited setting. Int J Emergency Med 11(1):8
17. Poggiali E et al (2020) “Can lung US help critical care clinicians in the early diagnosis of novel coronavirus (COVID-19) pneumonia?” Radiology, Mar. Art. no. 200847.
18. Peng Q-Y, Chinese Critical Care Ultrasound Study Group, Wang X-T, Zhang L-N (May 2020) Findings of lung ultrasonography of novel corona virus pneumonia during the 2019–2020 epidemic. Intensive Care Med 46(5):849–850
19. Soldati G et al (2020) “Is there a role for lung ultrasound during the COVID-19 pandemic?” J. Ultrasound Med.,
20. Soldati G et al (2020) “Proposal for international standardization of the use of lung ultrasound for patients with COVID-19: A simple, quantitative, reproducible method,” J. Ultrasound Med.,
21. Stefanidis K et al (2011) Lung sonography and recruitment in patients with early acute respiratory distress syndrome: A pilot study. Crit Care 15(4):R185
22. Stewart KA et al (2020) Trends in ultrasound use in low and middle income countries: A systematic review. Int J MCH AIDS 9(1):103–120
23. Tutino L, Cianchi G, Barbani F, Batacchi S, Cammelli R, Peris A (2010) Time needed to achieve completeness and accuracy in bedside lung ultrasound reporting in intensive care unit. Scandin J Trauma Resuscitation Emergency Med 18(1):44
24. Long L, Zhao H-T, Zhang Z-Y et al (2017) Lung ultrasound for the diagnosis of pneumonia in adults: a meta-analysis. Medicine 96:e5713
25. Lichtenstein DA, Mezière GA (2008) Relevance of lung ultrasound in the diagnosis of acute respiratory failure: the blue protocol. Chest 134:117–125
26. Ma OJ, Mateer JR (1997) Trauma ultrasound examination versus chest radiography in the detection of hemothorax. Ann Emerg Med 29:312–315
27. Buonsenso D, Pata D, Chiaretti A (2020) COVID-19 outbreak: less stethoscope, more ultrasound. Lancet Respir Med 8:e27

28. Dietrich CF, Mathis G, Blaivas M et al (2016) Lung B-line artefacts and their use. J Thorac Dis 8:1356–1365
29. Vinod DN, Prabaharan SRS (2020) Data science and the role of Artificial Intelligence in achieving the fast diagnosis of COVID-19. Chaos Solitons Fractals 140:110182
30. Born J, Brändle G, Cossio M, Disdier M, Goulet J, Roulin J, Wiedemann N (2020) POCOVID-Net: automatic detection of COVID-19 from a new lung ultrasound imaging dataset (POCUS). *arXiv preprint arXiv:2004.12084*
31. Simonyan K, Zisserman A (2014) Very deep convolutional networks for large-scale image recognition. *arXiv preprint arXiv:1409.1556*
32. Nitish Srivastava G, Hinton A, Krizhevsky I, Sutskever, Salakhutdinov R (2014) Dropout: a simple way to prevent neural networks from overfitting. J Mach Learn Res 15(1):1929–1958
33. Sergey Ioffe and Christian Szegedy (2015) Batch normalization: Accelerating deep network training by reducing internal covariate shift.arXiv preprintarXiv:1502.03167,
34. Born, J., Wiedemann, N., Cossio, M., Buhre, C., Brändle, G., Leidermann, K., … Borgwardt,K. (2021). Accelerating Detection of Lung Pathologies with Explainable Ultrasound Image Analysis. *Applied Sciences*, *11*(2), 672
35. Hu Z, Liu Z, Dong Y, Liu J, Huang B, Liu A, Zhou J (2021) Evaluation of lung involvement in COVID-19 pneumonia based on ultrasound images. Biomed Eng Online 20(1):1–15
36. Roy, S., Menapace, W., Oei, S., Luijten, B., Fini, E., Saltori, C., … Demi, L. (2020).Deep learning for classification and localization of COVID-19 markers in point-of-care lung ultrasound. *IEEE Transactions on Medical Imaging*, *39*(8), 2676–2687
37. https://github.com/DASARINAGAVINOD/COVID-19_Ultrasound.git
38. Zhou B, Khosla A, Lapedriza A, Oliva A, Torralba A (2016) Learning deep features for discriminative localization. In Proceedings of the IEEE Conference on Computer Vision and Pattern Recognition, Las Vegas, NV, USA, 27–30 June ; pp. 2921–2929
39. Selvaraju RR, Cogswell M, Das A, Vedantam R, Parikh D, Batra D (2017) Grad-cam: Visual explanations from deep networks via gradient-based localization. In Proceedings of the IEEE International Conference on Computer Vision, Venice, Italy, 22–29 October ; pp. 618–626
40. Khuzani AZ, Heidari M, Shariati SA (2021) COVID-Classifier: An automated machine learning model to assist in the diagnosis of COVID-19 infection in chest x-ray images. Sci Rep 11(1):1–6
41. Vinod DN, Jeyavadhanam BR, Zungeru AM, Prabaharan SRS(2021) Fully automated unified prognosis of COVID-19 chest X-ray/CT scan images using Deep Covix-Net model.*Computers in Biology and Medicine*,104729

Figures

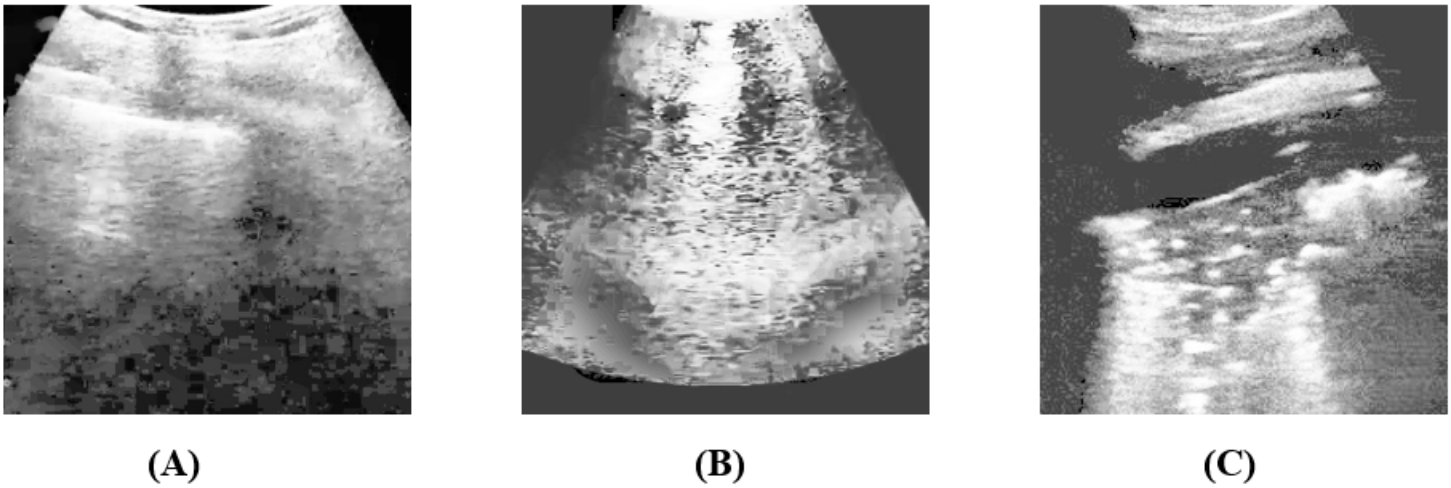

Figure 1

Sample lung ultrasound images of the database. (A) An exemplary COVID-19 contaminated lung, exhibiting small subpleural consolidation as well as pleural irregularities. (B) Healthy lung. (C) A Pneumonia contaminated lung, with dynamic air Broncho grams enclosed by alveolar consolidation.

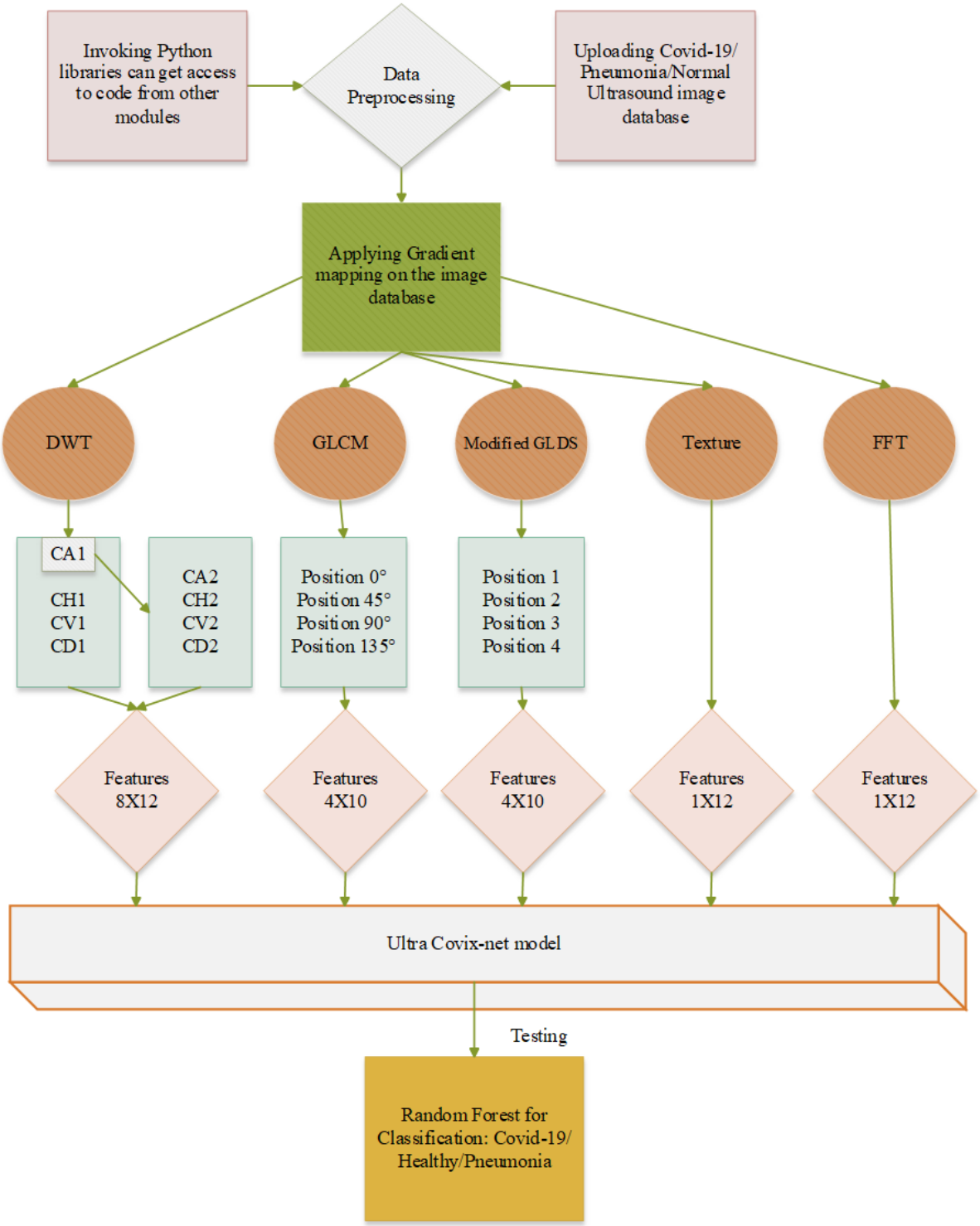

Figure 2

Taxonomy of the recommended mechanism to identify COVID-19/pneumonia/normal samples

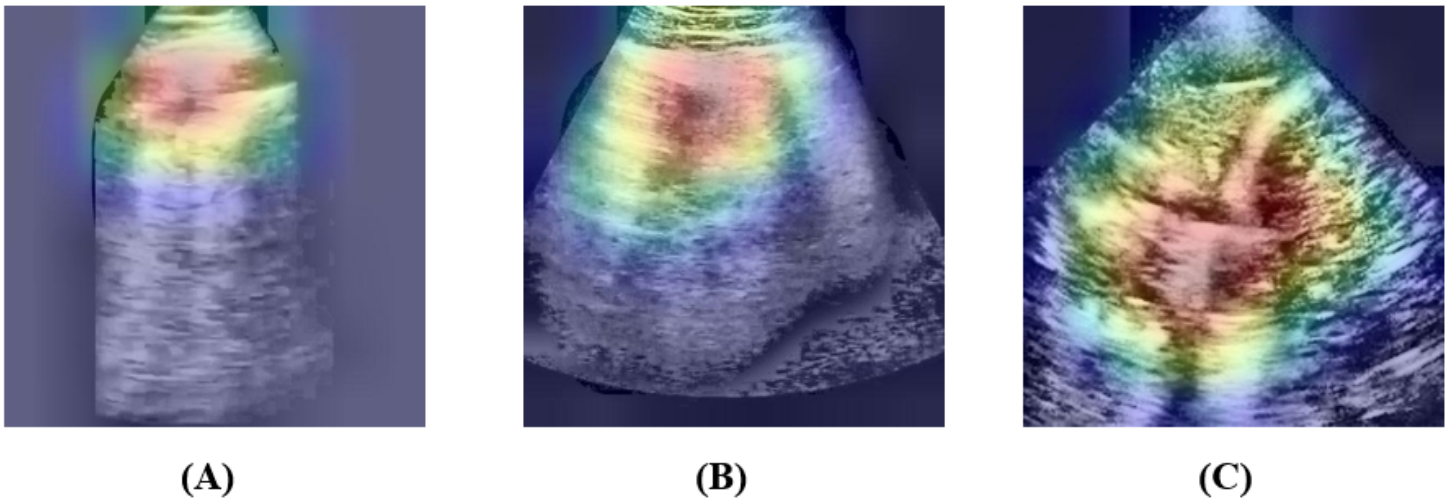

Figure 3

(A) Gradient mapping sample image of COVID-19 (highlighting B-line), (B) normal (highlighting A-lines), and (C) Pneumonia (highlighting Pleural consolidations)

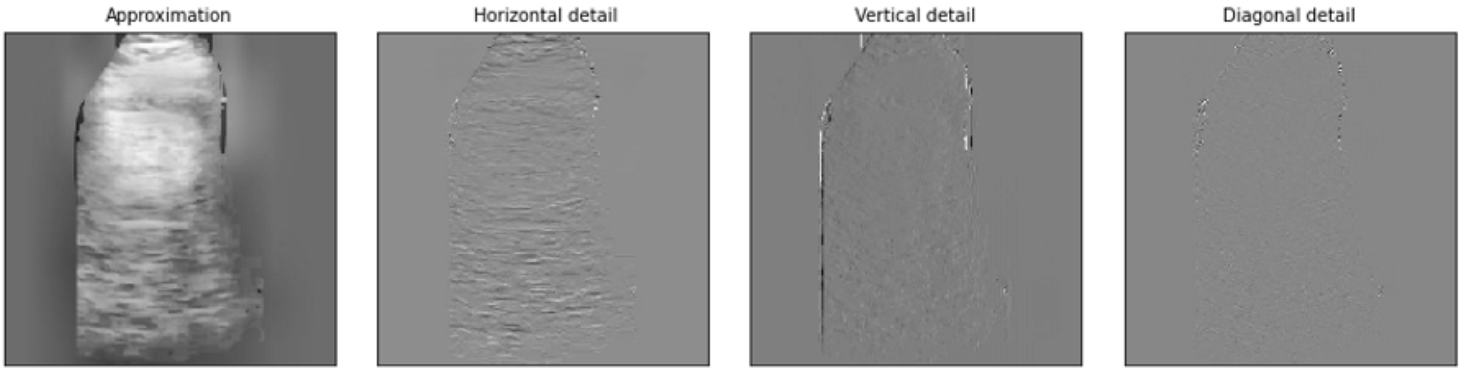

Figure 4

Wavelet transform mechanism on the slice of COVID-19 Ultrasound picture

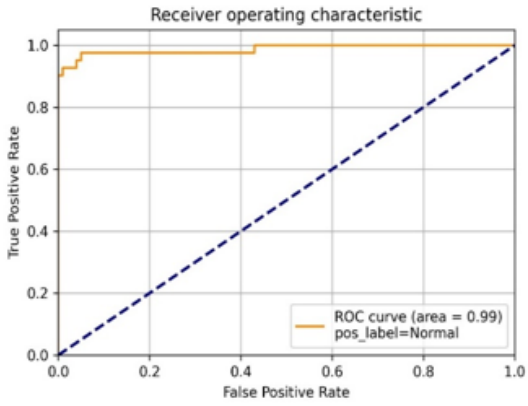

(a)

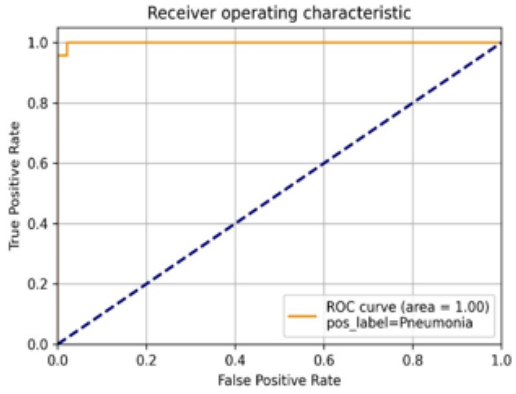

(b)

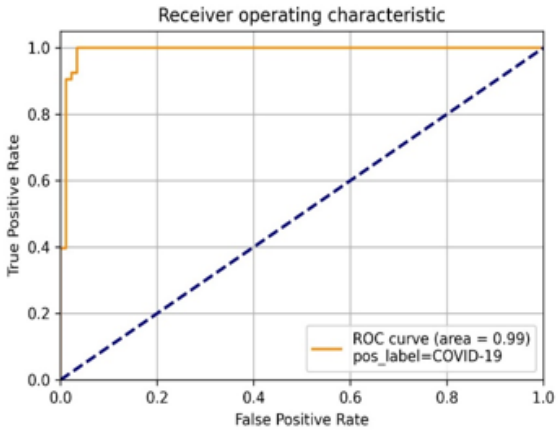

(c)

Figure 5

Ultrasound Image database performance- (a) Receiver Operating Characteristics graph provokes 211 test samples, amid Normal is the objective label. (b) Receiver Operating Characteristics graph provokes from 211 test samples, amid Pneumonia is the objective label. (c) Receiver Operating Characteristics graph provokes from 211 test samples, amid COVID-19 is the objective label.